

Impact of random and targeted disruptions on information diffusion during outbreaks

Hosein Masoomy,^{1, a)} Tom Chou,^{2, b)} and Lucas Böttcher^{3, c)}

¹⁾*Dept. of Physics, Shahid Beheshti University, 1983969411, Tehran, Iran*

²⁾*Depts. of Computational Medicine and Mathematics, UCLA, Los Angeles, CA 90095*

³⁾*Centre for Human and Machine Intelligence, Frankfurt School of Finance and Management, 60322 Frankfurt am Main, Germany*

(Dated: 3 January 2023)

Outbreaks are complex multi-scale processes that are impacted not only by cellular dynamics and the ability of pathogens to effectively reproduce and spread, but also by population-level dynamics and the effectiveness of mitigation measures. A timely exchange of information related to the spread of novel pathogens, stay-at-home orders, and other containment measures can be effective at containing an infectious disease, particularly during in the early stages when testing infrastructure, vaccines, and other medical interventions may not be available at scale. Using a multiplex epidemic model that consists of an information layer (modeling information exchange between individuals) and a spatially embedded epidemic layer (representing a human contact network), we study how random and targeted disruptions in the information layer (*e.g.*, errors and intentional attacks on communication infrastructure) impact outbreak dynamics. We calibrate our model to the early outbreak stages of the SARS-CoV-2 pandemic in 2020. Mitigation campaign can still be effective under random disruptions, such as failure of information channels between a few individuals. However, targeted disruptions or sabotage of hub nodes that exchange information with a large number of individuals can abruptly change outbreak characteristics such as the time to reach the peak infection. Our results emphasize the importance of using a robust communication infrastructure that can withstand both random and targeted disruptions.

Online communication platforms and exposure notification apps can help slow down and contain the spread of an infectious disease¹. Individuals who have been made aware of an outbreak are likely to adapt their behavior to reduce their risk of being infected. To study the interplay between infectious disease outbreaks and corresponding changes in individual contact behaviors, Granell *et al.*² introduced an epidemic model that accounts for the spread of awareness through an information layer that is coupled to a human contact network. Building upon their model of awareness diffusion, our work studies the impact of random and targeted disruptions in the information layer on the overall outbreak dynamics.

with progress in understanding epidemic processes in static single-layer networks, developments in the study of temporal networks¹⁷, multilayer networks^{18,19}, and other structures describing higher-order interactions^{20–23} have allowed for the integration of time-varying and non-binary interactions.

Before research turned to epidemic models in multilayer networks, interactions between disease and behavioral dynamics have been studied mainly in single-layer networks²⁴ and well-mixed populations.^{25–28} In an extension of the classical SIS model, the so-called susceptible-infected-alert-susceptible (SIAS) model, a new compartment was used to study the effect of “alert” individuals that are surrounded by a certain number of infecteds on disease dynamics.^{29,30} The SIAS model has been implemented using a two-layer network³¹ with a contact layer and an information-dissemination layer to find optimal information dissemination strategies that help contain an outbreak.

The interplay between behavioral effects and network dynamics has also been analyzed in terms of a multiplex structure where information on an outbreak diffuses in an information layer.^{2,32} In a multiplex network, all of the interlayer edges are edges between nodes and their counterparts in other layers. As in the SIAS model, individuals in the information layer can be either aware or unaware of a disease. Awareness then translates into a reduced infection rate. The original awareness model has been modified in various ways. One study used a threshold model in the information layer and identified awareness cascades.³³ Other research investigated the effects of dynamically varying transmission rates³⁴, coupled SIR and unaware-aware-unaware (UAU) dynamics with and without latency^{35,36}, SIS and UAU dynamics that propagate at different speeds³⁷, and higher-order interactions³⁸. For a detailed overview of models of coevolving spreading processes in networks, we refer the reader to Ref. 39.

I. INTRODUCTION

The study of epidemic processes in networks has provided many insights into the interplay between structure and dynamics.^{3,4} The aim of many works in this area has been to analyze the impact of different structural features such as clustering⁵, community structure^{6,7}, hub nodes, and scale-free degree distributions⁸ on the evolution of susceptible-infected-susceptible (SIS) and susceptible-infected-recovered (SIR) models and their extensions.^{9–11} Connections between epidemic processes and percolation contributed to the development of analytical methods that are useful to analyze epidemic transitions and determine outbreak size.^{12–16} Along

^{a)}hoseingmasoomy@gmail.com

^{b)}tomchou@ucla.edu

^{c)}l.boettcher@fs.de

In this work, we study coevolving susceptible-exposed-infected-recovered-deceased (SEIRD) and UAU dynamics on a multiplex network that consists of an epidemic layer and an information layer. The exposed compartment in our model accounts for latency (*i.e.*, the time difference between infection and becoming infectious). Different variants of SEIRD models have been used to mechanistically describe the spread of an infectious disease for which the latency period between time of infection to time of becoming infectious cannot be neglected^{9,40–42}. Examples of such infectious diseases include measles, smallpox, and SARS-CoV-2.

One of the main goals of this work is to provide insight into the impact of disruptions in the information diffusion layer on the overall outbreak dynamics. We therefore study different edge removal protocols that describe random and targeted disruptions. In Sec. II, we define the disease and awareness model, develop a heterogeneous mean-field model, define random and targeted edge removal protocols, and briefly describe the structure of the considered networks. In Sec. III, we first discuss a baseline simulation that uses model parameters that are aligned with empirical data on the outbreak of SARS-CoV-2 in early 2020. We then use this baseline simulation as a reference to study the impact of disruptions in the information diffusion layer on three disease severity measures: (i) final outbreak size, (ii) maximum proportion of infectious nodes on a given day (*i.e.*, the height of the infection peak), and (iii) the time until the infection peak is reached.

II. METHODS

A. Epidemic model with information diffusion

We study the interplay between information diffusion and epidemic dynamics in a multiplex network with two layers [see Fig. 1(a)].

In the first layer, individuals exchange information (*e.g.*, through online social media or messaging services) on the prevalence of a certain disease in the overall population according to the unaware-aware-unaware (UAU) model.² Individuals in the “information layer” (IL) can be in two states. They are either unaware (U) or aware (A) of the disease and do not necessarily have to be in close proximity (in terms of connectivity) to exchange information. Unaware nodes can become aware in two ways. First, if an unaware node is in contact with an aware node, it becomes aware at rate λ . Second, nodes that have been infected and experience symptoms become aware at rate κ . Given that certain individuals forget or do not adhere to intervention measures after a certain time, we also account for transitions from aware to unaware at rate δ . A schematic of UAU dynamics is shown in Fig. 1(b).

In the second layer, we model an epidemic outbreak using the susceptible-exposed-infected-recovered-deceased (SEIRD) model. In the “epidemic layer” (EL), nodes can be in states S (susceptible), E (exposed), I (infected), R (recovered), and D (deceased). We distinguish between two infection rates, β^u and β^a , that describe the rates at which susceptible nodes become infected if they are unaware and aware, respectively.

The disease transmission rate associated with aware individuals is assumed to be strictly lower than the disease transmission rate associated with unaware individuals (*i.e.*, $\beta^a < \beta^u$), accounting for the decreased likelihood of an aware individual to become infected. We assume a latent rate σ , resolution rate γ , and infection fatality ratio f that are independent of the awareness status. This assumption is valid for infectious diseases for which no medication is available that positively affects recovery, even if a person is aware of an infection before developing symptoms. For example, during the early outbreak stages of SARS-CoV-2, there was very little information available on how to medically support patients that were aware of their infection, but did not show symptoms yet. Non-pharmaceutical interventions such as contact restrictions, mask mandates, and quarantine are often the only possibility to combat novel pathogens.¹

According to the described UAU and SEIRD dynamics, nodes can be in the following states: (U, S) , (A, S) , (U, E) , (A, E) , (U, I) , (A, I) , (U, R) , (A, R) , and (U, D) . The first entry in each tuple describes the awareness state (either U or A) while the second entry describes vital and disease states (S, E, I, R , and D). Deceased nodes are not aware.

B. Heterogeneous mean-field theory

In accordance with Ref. 43, we formulate a heterogeneous mean-field theory of SEIRD-UAU dynamics. We use $x_j y_k(t)$ ($x \in \{u, a\}, y \in \{s, e, i, r, d\}$) to denote the proportion of nodes in state $X_j Y_k$ ($X \in \{U, A\}, Y \in \{S, E, I, R, D\}$) with degrees j and k in the IL and EL at time t , respectively. For example, $u_j s_k \equiv u_j s_k(t)$ denotes the proportion of unaware and susceptible nodes with degrees j and k in the IL and EL at time t , respectively. Henceforth, we will not explicitly include the time dependence in the notation $x_j y_k$ for the sake of notational brevity.

The proportions of susceptible, exposed, infected, recovered, and deceased nodes are

$$s_k = \sum_{j=1}^J (u_j s_k + a_j s_k), \quad (1)$$

$$e_k = \sum_{j=1}^J (u_j e_k + a_j e_k), \quad (2)$$

$$i_k = \sum_{j=1}^J (u_j i_k + a_j i_k), \quad (3)$$

$$r_k = \sum_{j=1}^J (u_j r_k + a_j r_k), \quad (4)$$

$$d_k = \sum_{j=1}^J u_j d_k, \quad (5)$$

where J is the maximum (or cut-off) degree in the IL. Similarly, we find that the proportions of unaware and aware nodes

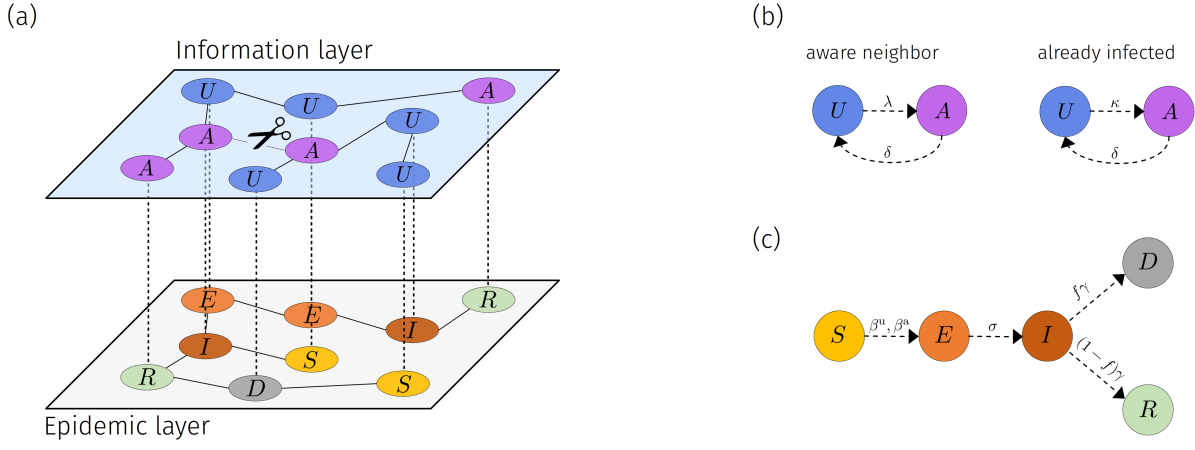


FIG. 1. Model schematic. (a) Information layer and epidemic layer. Nodes in the information layer are either unaware (U) or aware (A) while nodes in the epidemic layer can be in one of five different states: susceptible (S), exposed (E), infected (I), recovered (R), and deceased (D). Edge removal that is caused by disruptions in the information layer is indicated by the scissor symbol. (b) Unaware nodes become aware at rate λ if they are adjacent to an aware node. If unaware nodes are infected, they can also become aware at rate κ . Aware nodes transition back to an unaware state at rate δ . (c) Infectious nodes transmit a disease to unaware and aware susceptible nodes at rates β^u and β^a , respectively. To account for a reduction in infectiousness risk of aware nodes, we assume the value of the disease transmission rate β^u associated with unaware nodes is strictly larger than the value of the disease transmission rate β^a associated with aware nodes ($\beta^u > \beta^a$). Once susceptible nodes have been infected, they enter an exposed state and become infectious at rate σ . The characteristic time scale σ^{-1} corresponds to the latency period of the disease. Infected nodes either die or recover at rates $f\gamma$ and $(1-f)\gamma$, respectively.

are

$$u_j = \sum_{k=1}^K (u_j s_k + u_j e_k + u_j i_k + u_j r_k + d_k), \quad (6)$$

$$a_j = \sum_{k=1}^K (a_j s_k + a_j e_k + a_j i_k + a_j r_k), \quad (7)$$

where K is the maximum (or cut-off) degree in the EL. These quantities satisfy the normalization conditions

$$\sum_{k=1}^K (s_k + e_k + i_k + r_k + d_k) = 1, \quad (8)$$

$$\sum_{j=1}^J (u_j + a_j) = 1. \quad (9)$$

Assuming an uncorrelated network⁴⁴, the rate equations of the heterogeneous mean-field model are

$$\frac{du_j s_k}{dt} = -\lambda \frac{ju_j s_k}{\langle \tilde{k} \rangle} \sum_{j'} j' a_{j'} - \beta^u \frac{ku_j s_k}{\langle k \rangle} \sum_{k'} k' i_{k'} + \delta a_j s_k, \quad (10)$$

$$\frac{da_j s_k}{dt} = \lambda \frac{ju_j s_k}{\langle \tilde{k} \rangle} \sum_{j'} j' a_{j'} - \beta^a \frac{ka_j s_k}{\langle k \rangle} \sum_{k'} k' i_{k'} - \delta a_j s_k, \quad (11)$$

$$\begin{aligned} \frac{du_j e_k}{dt} = & -\lambda \frac{ju_j e_k}{\langle \tilde{k} \rangle} \sum_{j'} j' a_{j'} + \beta^u \frac{ku_j s_k}{\langle k \rangle} \sum_{k'} k' i_{k'} \\ & - \sigma u_j e_k + \delta a_j e_k \end{aligned} \quad (12)$$

and

$$\begin{aligned} \frac{da_j e_k}{dt} = & \lambda \frac{ju_j e_k}{\langle \tilde{k} \rangle} \sum_{j'} j' a_{j'} + \beta^a \frac{ka_j s_k}{\langle k \rangle} \sum_{k'} k' i_{k'} \\ & - \sigma a_j e_k - \delta a_j e_k, \end{aligned} \quad (13)$$

$$\begin{aligned} \frac{du_j i_k}{dt} = & -\lambda \frac{ju_j i_k}{\langle \tilde{k} \rangle} \sum_{j'} j' a_{j'} + \sigma u_j e_k - \gamma u_j i_k \\ & - \kappa u_j i_k + \delta a_j i_k, \end{aligned} \quad (14)$$

$$\begin{aligned} \frac{da_j i_k}{dt} = & \lambda \frac{ju_j i_k}{\langle \tilde{k} \rangle} \sum_{j'} j' a_{j'} + \sigma a_j e_k - \gamma a_j i_k \\ & + \kappa u_j i_k - \delta a_j i_k, \end{aligned} \quad (15)$$

$$\frac{du_j r_k}{dt} = -\lambda \frac{ju_j r_k}{\langle \tilde{k} \rangle} \sum_{j'} j' a_{j'} + (1-f)\gamma u_j i_k + \delta a_j r_k, \quad (16)$$

$$\frac{da_j r_k}{dt} = \lambda \frac{ju_j r_k}{\langle \tilde{k} \rangle} \sum_{j'} j' a_{j'} + (1-f)\gamma a_j i_k - \delta a_j r_k, \quad (17)$$

$$\frac{du_j d_k}{dt} = f\gamma (u_j + a_j) i_k, \quad (18)$$

where $\langle k \rangle$ and $\langle \tilde{k} \rangle$ denote the mean degrees of the EL and IL, respectively.

C. Networks

In our numerical experiments, we use a Barabási–Albert (BA) network⁴⁵ to model the information layer of the two-layer structure underlying SEIRD-UAU dynamics. Such networks exhibit scale-free degree distributions $p(k) \propto k^{-\gamma}$

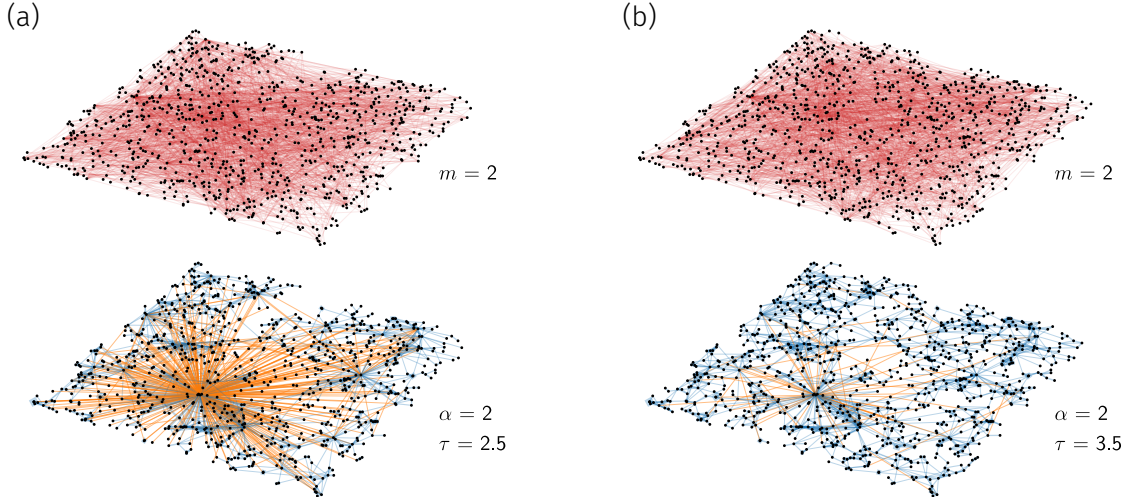


FIG. 2. Multiplex networks. Information layer (top layer) with BA structure and epidemic layer (bottom layer) with GIRG structure determined by exponents $\alpha = 2$, $\tau = 2.5$ (a) and $\alpha = 2$, $\tau = 3.5$ (b). In the BA network, each new node has $m = 2$ edges that connect it to existing nodes using linear preferential attachment. We use blue and orange edges in the epidemic layer to indicate short-range and long-range connections, respectively. An edge connecting two nodes i, j is considered a short-range connection if the corresponding positions $\mathbf{x}_i, \mathbf{x}_j$ satisfy $\|\mathbf{x}_i - \mathbf{x}_j\| < 7$. Otherwise, it is considered a long-range connection. The numbers of nodes in panels (a) and (b) are $N = 921$ and $N = 973$, respectively.

($\gamma > 0$), and are often found in social and technological systems.^{46–50} Note that other distributions such as log-normal distributions may also provide good descriptions of empirical degree distributions in seemingly scale-free networks.⁵¹ In the epidemic layer, we use a geometric inhomogeneous random graph (GIRG)⁵², a spatial network that has found applications in representing spatially embedded metapopulation structures in COVID-19 models.⁵³

1. Barabási–Albert network

Barabási–Albert networks⁴⁵ are constructed using a preferential attachment procedure in which new nodes that are iteratively added to an existing network have a higher likelihood of being attached to nodes that have higher numbers of connections. A mean field analysis of the BA model and corresponding numerical results show that the exponent of the power-law degree distribution is $\gamma \approx 3$.⁵⁴

To construct the BA network that we will use in our simulations, we start with a star graph with one root node and two leave nodes and iteratively add new nodes until we reach N nodes. Each new node has $m = 2$ edges that connect it to existing nodes using linear preferential attachment. A visualization of such a BA information layer network with $N \approx 10^3$ is given in the top row of Fig. 2. In our simulations, we use a BA network with a larger node number of $N \approx 10^4$ that is constructed in the same way as the ILs in Fig. 2.

2. Geometric inhomogeneous random graph

The GIRG model^{52,55} produces a spatially embedded scale-free random network. In this model, N points are first selected uniformly at random in the n -dimensional hypercube $K^n = [0, 1]^n$. We denote the randomly selected point positions by $\mathbf{x}_i \in K^n$ ($1 \leq i \leq N$) and assign each of them a weight w_i whose value is drawn from a power-law distribution $\tilde{p}(w) = (\tau - 2)w^{-\tau}$ ($w \geq 1, \tau \geq 2$).^{52,55} Note that the distribution $\tilde{p}(w)$ is normalized such that its mean value is equal to 1. Pairs of nodes i, j with positions $\mathbf{x}_i, \mathbf{x}_j$ are adjacent with probability

$$\Pi_{ij} = 1 - \exp \left[- \left(\frac{w_i w_j}{\|\mathbf{x}_i - \mathbf{x}_j\|^n} \right)^\alpha \right], \quad (19)$$

where $\|\mathbf{x}_i - \mathbf{x}_j\|$ denotes the Euclidean distance between points \mathbf{x}_i and \mathbf{x}_j . The resulting degrees k_i ($1 \leq i \leq N$) are also distributed according to a power law with exponent τ .

According to Eq. 19, the exponent α tunes the distance and weight dependence of Π_{ij} . For $\alpha = 0$, the probability that two nodes i, j are adjacent is independent of their distance $|\mathbf{x}_i - \mathbf{x}_j|$. That is, $\Pi_{ij} = 1 - e^{-1}$ for all i, j . By increasing α , the distance-dependence of Π_{ij} strongly influences the structure of the network so that only nearby nodes are likely to be adjacent. The bottom row of Fig. 2 shows GIRGs for various parameters.

For small exponents $\tau \geq 2$, the number of nodes with large weight values increases. According to Eq. 19, nodes with large weights are more likely to be connected than nodes with

small weights. The abundance of these large-weight nodes, which are the hubs of the underlying scale-free network, impacts the global structure of GIRG. By decreasing τ , many long-range connections are added to the GIRG. In the bottom row of Fig. 2, we observe that smaller values of τ are associated with a larger proportion of long-range connections.

D. Edge removal

To model disruptions in the IL, we consider two different edge-removal protocols: (i) random edge removal and (ii) targeted edge removal. In both protocols, we select $\tilde{N} \leq N$ nodes and denote the proportion of selected nodes by $q = \tilde{N}/N$. For each selected node, we remove each of its edges with probability p . Values of $p, q > 0$ correspond to disruptions in the IL that slow down the information spread. For $p = q = 1$, there are no awareness dynamics and the epidemic progresses without interference from the information layer.

In random edge removal, \tilde{N} nodes are selected uniformly at random while we select \tilde{N} hub nodes (*i.e.*, nodes with the largest degrees) in targeted edge removal. Such random and targeted disruptions have been studied to provide insight into the ability of different types of networks to withstand errors and intentional attacks.⁶⁵ It has been shown that structural features of scale-free networks such as the size of the largest connected component are very sensitive to intentional attacks (or sabotage).^{66,67}

We next explore how variations in $p, q \in [0, 1]$ impact the total proportion of infections $i^* = 1 - s^*$, peak infection (*i.e.*, the maximum proportion of the population that was infected on any day), and the time between the beginning of the outbreak until peak infection is reached.

III. RESULTS

First consider a baseline case of SEIRD-UAU dynamics without edge removal (*i.e.*, $pq = 0$) in two different multiplex networks. Both multiplex networks are connected and have the same BA information layer (see Sec. II C 1). In the epidemic layer, we set $\tau = 3.5$ and $\tau = 2.5$ to model contact networks with different proportions of long-range connections (see Fig. 2). In the remainder of this work, we will refer to the networks with $\tau = 2.5$ and $\tau = 3.5$ as long-range and short-range networks, respectively. In both networks, we set $\alpha = 2$ [see Eq. (19)]. All stochastic simulations are implemented using Gillespie's algorithm.^{68–70}

A. Baseline

We have chosen the model parameters that we use in the baseline simulation in accordance with empirical data on the outbreak of SARS-CoV-2 in the beginning of 2020. For example, for the two multiplex networks that we use in our simulations, we have set the infection rate of unaware nodes to $\beta^u = 0.17, 0.6 \text{ day}^{-1}$ to obtain a basic reproduction number R_0

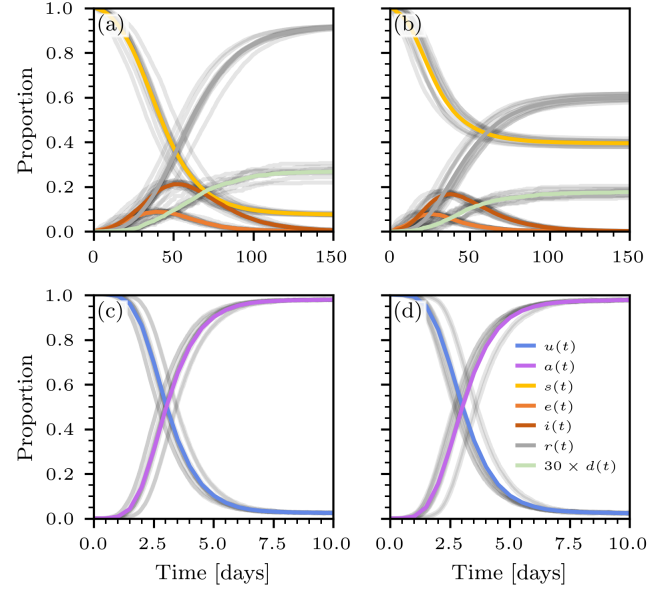


FIG. 3. Stochastic simulation of baseline scenario without information-layer disruption (*i.e.*, $pq = 0$). (a,b) Proportions of susceptible ($s(t)$), exposed ($e(t)$), infected ($i(t)$), recovered ($r(t)$), and deceased ($d(t)$) nodes at time t . The exponent τ in the epidemic layer in panels (a,c) and (b,d) is set to 3.5 (short range) and 2.5 (long range), respectively. The corresponding numbers of nodes are $N = 10049$ and $N = 10025$. Solid colored lines represent mean values that are based on 10 i.i.d. realizations (thin grey lines).

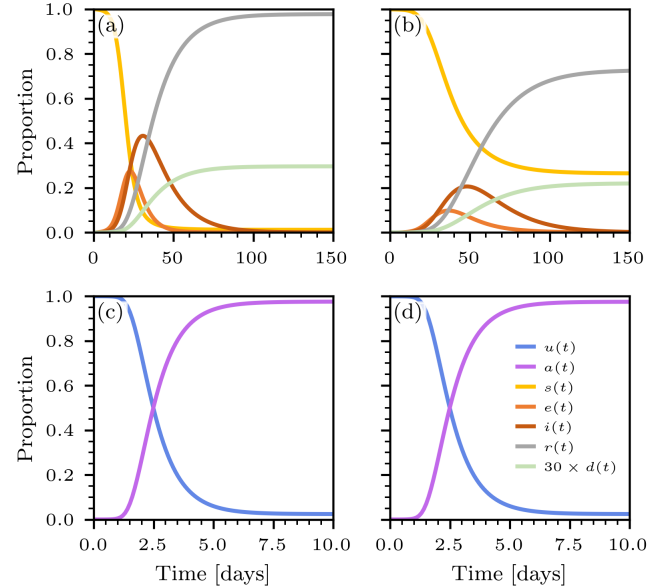


FIG. 4. Heterogeneous mean-field solution of baseline scenario without information-layer disruption (*i.e.*, $pq = 0$). (a,b) Proportions of susceptible ($s(t)$), exposed ($e(t)$), infected ($i(t)$), recovered ($r(t)$), and deceased ($d(t)$) nodes at time t . The exponent τ in the epidemic layer in panels (a,c) and (b,d) is set to 3.5 (short range) and 2.5 (long range), respectively. The corresponding numbers of nodes are $N = 10049$ and $N = 10025$.

Parameter	Symbol	Value	Units	Comments/references
Infection rate (unaware)	β^u	0.17, 0.6	day ⁻¹	inferred from $R_0 \approx 2 - 4$ for a given $\gamma^{56,57}$
Infection rate (aware)	β^a	$0.2\beta^u$	day ⁻¹	58
Latent rate	σ	1/5	day ⁻¹	59
Resolution rate	γ	1/14	day ⁻¹	60,61
Infection fatality ratio	f	1%	...	62,63
Awareness rate (infected)	κ	1	day ⁻¹	64
Base awareness rate	λ	0.5κ	day ⁻¹	64
Unawareness rate	δ	1/30	day ⁻¹	64

TABLE I. Overview of model parameters. We use infection rates $\beta^u = 0.17 \text{ day}^{-1}$ and $\beta^a = 0.6 \text{ day}^{-1}$ for GIRG networks with $\tau = 2.5$ (long range) and $\tau = 3.5$ (short range), respectively.

of about $2 - 4$.^{56,57} Given a latency period of about 5 days⁵⁹, we set the latent rate to $\sigma = 1/5 \text{ day}^{-1}$. The resolution rate is set to $\gamma = 1/14 \text{ day}^{-1}$, and we use an infection fatality ratio f of 1%.⁶⁰⁻⁶³ Other model parameters that are associated with UAU dynamics are as in Ref. 64. We provide an overview of all parameters and corresponding references in Tab. I.

Figure 3 shows the stochastic evolution of the proportions of susceptible $s(t)$, exposed $e(t)$, infected $i(t)$, recovered $r(t)$, and deceased $d(t)$ nodes in the EL and of unaware $u(t)$ and aware $a(t)$ nodes in the IL. Initially, 10 nodes are infectious and 1 node is aware. For networks of about $N = 10000$ nodes that are used in our stochastic simulations, these initial conditions correspond to $i(0) \approx 10^{-3}$ and $a(0) \approx 10^{-4}$. The simulation results shown in Figs. 3(a,c) and Figs. 3(b,d) are based on short-range ($\tau = 3.5$) and long-range ($\tau = 2.5$) GIRGs, respectively. The evolution of the UAU dynamics in the IL is very similar for both GIRGs. However, structural differences between the ELs directly impact the evolution of SEIRD dynamics. The infected fraction peaks at ~ 0.17 after about 38 days in the long-range EL but peaks at ~ 0.21 at about 51 days in the short-range EL. Figure 3 also shows that the final epidemic size $1 - s(t \rightarrow \infty)$ in both networks differs significantly. To understand what causes the different outbreak characteristics in both networks, we examined the degree distribution of susceptible nodes at $T = 150$: there are substantially more susceptible low-degree nodes in the long-range GIRG where $\tau = 2.5$ compared to the short-range GIRG with $\tau = 3.5$. Although, there are more hub nodes with large degree in the long-range GIRG, the proportion of low-degree nodes is also larger. Hence, there are more low-degree nodes in the long-range GIRG that are less exposed to the outbreak dynamics.

To complement the stochastic simulation results, we numerically solve the heterogeneous mean-field model (10)-(18) for the same networks and model parameters (see Tab. I). We set the degree cut-offs to $J = 210$, $K = 400$ ($\tau = 2.5$) and $J = 210$, $K = 164$ ($\tau = 3.5$). In the multiplex network with short-range IL with $\tau = 3.5$, the degree cut-offs correspond to the maximum degrees. In the long-range EL where $\tau = 2.5$, the maximum degree is 856, and to keep the solution of the mean-field model computationally feasible we set

the cut-off $K = 400$. Initially, we set $a_j i_k(0) = p_j \tilde{p}_k a(0)/2$, $a_j s_k(0) = p_j \tilde{p}_k a(0)/2$, $u_j s_k(0) = p_j \tilde{p}_k (1 - i(0) - a(0))/2$, $u_j i_k(0) = p_j \tilde{p}_k (i(0) - a(0)/2)$, where p_j and \tilde{p}_k denote the degree distributions in the IL and EL, respectively. Both degree distributions are normalized according to $\sum_{j=1}^J p_j = 1$ and $\sum_{k=1}^K \tilde{p}_k = 1$.

Note that these initial conditions satisfy

$$s(0) = \sum_{j,k} (u_j s_k(0) + a_j s_k(0)) \quad (20)$$

$$= \sum_{j,k} p_j \tilde{p}_k [1 - i(0)] = 1 - i(0), \quad (21)$$

$$i(0) = \sum_{j,k} (u_j i_k(0) + a_j i_k(0)) = \sum_{j,k} p_j \tilde{p}_k i(0), \quad (22)$$

$$u(0) = \sum_{j,k} (u_j s_k(0) + u_j i_k(0)) \quad (23)$$

$$= \sum_{j,k} p_j \tilde{p}_k [1 - a(0)] = 1 - a(0), \quad (24)$$

$$a(0) = \sum_{j,k} (a_j s_k(0) + a_j i_k(0)) = \sum_{j,k} p_j \tilde{p}_k a(0). \quad (25)$$

In accordance with the initial conditions that we used in the stochastic simulations, we set $i(0) = 10^{-3}$ and $a(0) = 10^{-4}$. Figure 4 shows the corresponding numerical results. Comparing Figs. 3 to 4, we observe that the heterogeneous mean-field model captures characteristic features that arise in the evolution of stochastic SEIRD-UAU dynamics. Examples of such features include (i) the rapid spread of awareness in the IL and (ii) differences between both ELs in the final epidemic size $1 - s(t \rightarrow \infty)$. In the heterogeneous mean-field model (10)-(18), we account only for differences in node degree and neglect other structural features of the considered multiplex networks. Subpopulations interact in a well-mixed manner and susceptible nodes of the same degree have the same risk of being infected at any given time. As a consequence of these approximations, the mean-field model overestimates both the number of new infections and final outbreak size compared to the stochastic simulation results in Fig. 3.

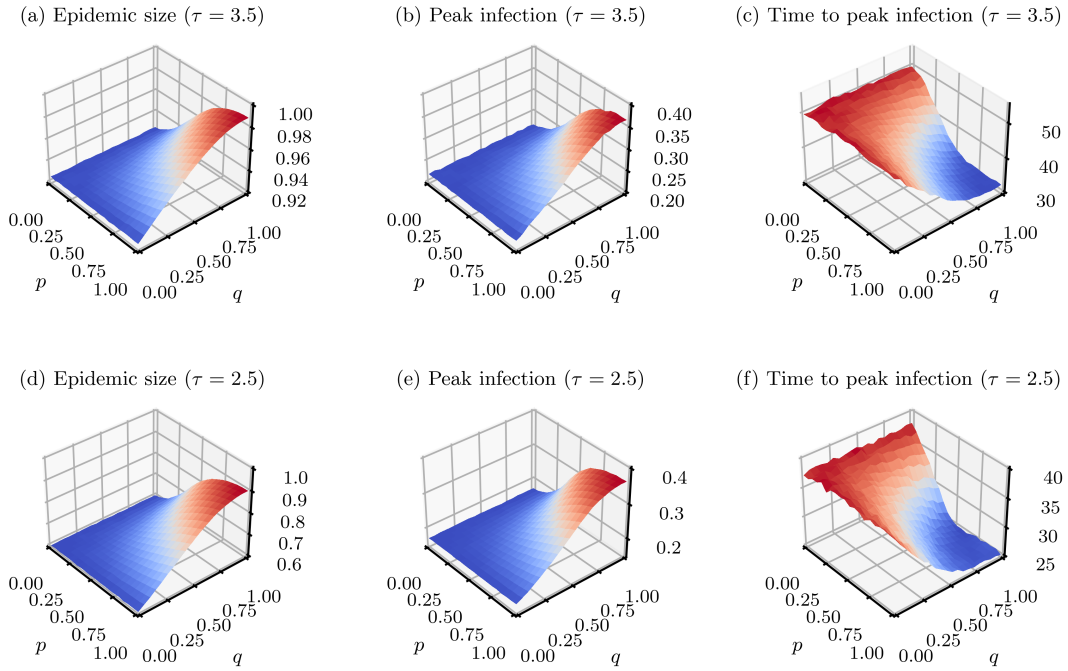


FIG. 5. Random edge removal. The impact of random edge removal in the IL on disease dynamics in the EL. Epidemic size $1 - s(t \rightarrow \infty)$ (left column), peak infection (middle column), and time to peak infection (right column) as a function of the proportion of selected nodes q and the corresponding edge removal probability p . The exponent τ in the ELs in top row and bottom row is set to 3.5 (short range) and 2.5 (long range), respectively. The corresponding numbers of nodes are $N = 10049$ and $N = 10025$. Simulation results are based on 230 i.i.d. realizations.

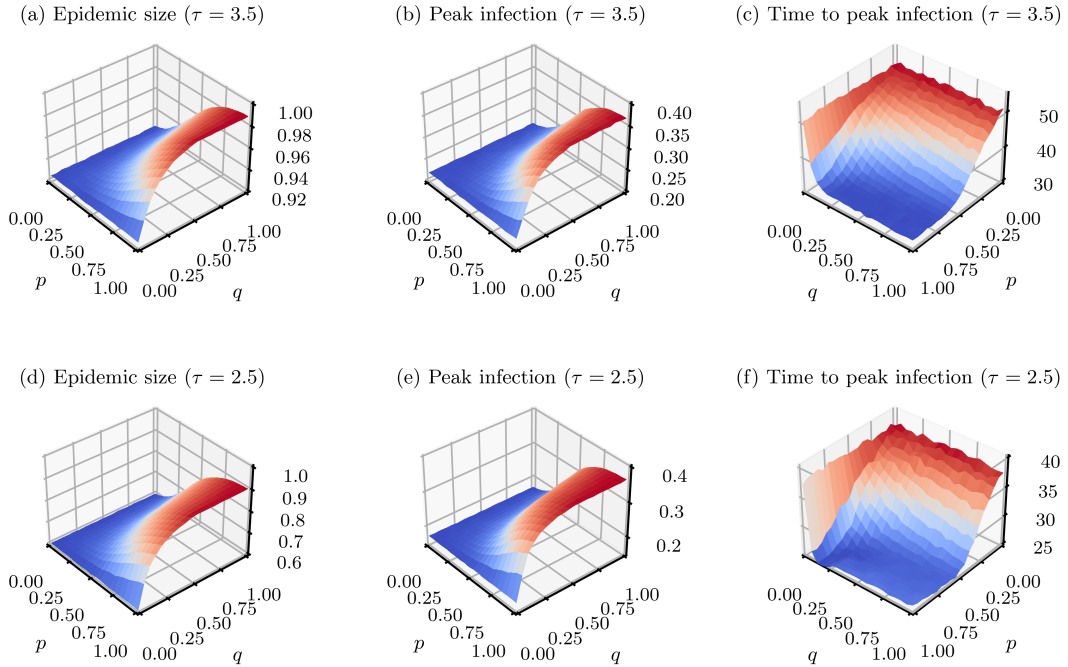


FIG. 6. Targeted edge removal. The impact of random edge removal in the IL on disease dynamics in the EL. Epidemic size $1 - s(t \rightarrow \infty)$ (left panel), peak infection (middle panel), and time to peak infection (right panel) as a function of the proportion of selected nodes q and the corresponding edge removal probability p . The exponent τ in the ELs in top row and bottom row is set to 3.5 (short range) and 2.5 (long range), respectively. The corresponding numbers of nodes are $N = 10049$ and $N = 10025$. Simulation results are based on 230 i.i.d. realizations.

B. Impact of edge removal

We now study the impact of random and targeted edge removal in the IL (see Sec. IID) on SEIRD dynamics in terms of three disease severity measures: (i) final epidemic size, (ii) peak infection, and (iii) time to peak infection.

1. Random edge removal

In random edge removal, we first select a proportion of $q = \tilde{N}/N$ nodes in the IL uniformly at random. For each of the selected nodes, each of its edges are removed with probability p .

Figure 5(a,d) shows the epidemic size as a function of p, q for both short-range and long-range GIRGs. The epidemic size increases with p and q because larger values of p, q are associated with fewer edges in the IL, leading to a smaller proportion of aware nodes. Hence, the proportion of nodes with a reduced infection rate β^u also decreases. For the long-range GIRG ($\tau = 2.5$), the final epidemic size undergoes a transition from about 0.6 for $p, q \approx 0$ to about 0.9 for $p, q \approx 1$. Because the final epidemic size in the short-range GIRG ($\tau = 3.5$) is already about 0.9, random edge removal has relatively little impact on this quantity.

As with the impact on final epidemic size $1 - s(t \rightarrow \infty)$, random edge removal generates a similar-looking p, q -dependent infection peak, as shown in Fig. 5(b,e). The time to reach peak infection decreases with p, q since higher p, q are associated with smaller proportions of aware nodes. Thus, the proportion of nodes with a reduced infection rate β^u also decreases, and the epidemic spreads faster through the network.

2. Targeted edge removal

For targeted edge removal where the \tilde{N} selected nodes correspond to the hubs (*i.e.*, largest-degree nodes) of the IL, we find that the overall dependence of epidemic size, peak infection, and time to peak infection on p, q is qualitatively similar to random edge removal (see Fig. 6). As in random edge removal, the impact of targeted edge removal on the final epidemic size is smaller for the short-range GIRG compared to the long-range one. A key difference in targeted edge removal is that all studied quantities are more sensitive to variations in q , the proportion of selected hub nodes. For example, the transition of the epidemic size for $p = 1$ as a function of q in targeted edge removal [see Fig. 6(a,d)] is steeper than the corresponding transition in random edge removal [see Fig. 5(a,d)].

Targeted edge removal selects nodes based on their degree rather than uniformly, and leads to more significant changes in epidemic size, peak infection, and time to peak infection as $p \geq 0.5$. These findings are in accordance with previous work that showed that scale-free networks break down more easily under intentional attacks than under uniform random failure.⁶⁷ Our work provide insights into how such disruptions in information diffusion translate into differences in disease severity measures.

IV. DISCUSSION

In this work, we studied the impact of disruptions in communication networks on information diffusion and subsequently disease outcome during an outbreak. To do so, we constructed a multiplex network that consists of two layers. The first layer, called information layer (IL), is used to model communication between individuals (*e.g.*, online information exchange via a social media platform). The second layer, called epidemic layer (EL), is used to represent a spatially embedded human contact network in which infectious individuals can transmit a disease to susceptible individuals. We use this multiplex network to simulate coevolving unaware-aware-unaware (UAU) and susceptible-exposed-infected-recovered-deceased (SEIRD) dynamics. The model parameters that we use in our simulations have been selected in accordance with empirical data on the early outbreak stages of SARS-CoV-2 in the beginning of 2020.

We studied two different epidemic layers with different proportions of long-range connections, representing human contact networks with different contact characteristics. To illustrate the impact of disruptions in the IL on the evolution of an outbreak, we utilized two different edge removal protocols: (i) random edge removal and (ii) targeted edge removal. In both protocols, we select a proportion q of nodes and then remove corresponding edges with probability p . In random edge removal, we select nodes in the IL uniformly at random while we select nodes with the largest degree (*i.e.*, hub nodes) in targeted edge removal. Although edge removal may render the IL disconnected, the EL is always connected in our simulations such that all nodes in the EL can potentially be infected. Previous work has shown that scale-free networks such as the IL in our multiplex network are more robust to random than targeted disruptions.⁶⁵⁻⁶⁷ The reason for this effect is that by removing hub nodes of a scale-free network, a large number of all edges in the network is being removed, strongly impacting the connectivity properties of such a network. We observe that targeted edge removal can abruptly change outbreak characteristics such as time to peak infection, even for small proportions of selected nodes. Our results extend those presented in previous work on random and targeted disruptions⁶⁵⁻⁶⁷ by establishing a connection to coevolving information and epidemic diffusion.

DATA AVAILABILITY

Our source codes are publicly available at <https://gitlab.com/ComputationalScience/information-epidemic>.

¹T. Schneider, O. R. Dunbar, J. Wu, L. Böttcher, D. Burov, A. Garbuno-Inigo, G. L. Wagner, S. Pei, C. Daraio, R. Ferrari, *et al.*, “Epidemic management and control through risk-dependent individual contact interventions,” *PLOS Computational Biology* **18**, e1010171 (2022).

²C. Granell, S. Gómez, and A. Arenas, “Dynamical interplay between awareness and epidemic spreading in multiplex networks,” *Physical Review Letters* **111**, 128701 (2013).

³J. P. Gleeson, “Binary-state dynamics on complex networks: Pair approximation and beyond,” *Physical Review X* **3**, 021004 (2013).

- ⁴R. Pastor-Satorras, C. Castellano, P. Van Mieghem, and A. Vespignani, "Epidemic processes in complex networks," *Reviews of Modern Physics* **87**, 925 (2015).
- ⁵M. E. J. Newman, "Properties of highly clustered networks," *Physical Review E* **68**, 026121 (2003).
- ⁶W. Huang and C. Li, "Epidemic spreading in scale-free networks with community structure," *Journal of Statistical Mechanics: Theory and Experiment* **2007**, P01014 (2007).
- ⁷I. Tunc and L. B. Shaw, "Effects of community structure on epidemic spread in an adaptive network," *Physical Review E* **90**, 022801 (2014).
- ⁸R. Pastor-Satorras and A. Vespignani, "Epidemic spreading in scale-free networks," *Physical Review Letters* **86**, 3200 (2001).
- ⁹M. J. Keeling and P. Rohani, *Modeling infectious diseases in humans and animals* (Princeton University Press, 2011).
- ¹⁰L. Böttcher, O. Woolley-Meza, E. Goles, D. Helbing, and H. J. Herrmann, "Connectivity disruption sparks explosive epidemic spreading," *Physical Review E* **93**, 042315 (2016).
- ¹¹L. Böttcher, H. J. Herrmann, and M. Henkel, "Dynamical universality of the contact process," *Journal of Physics A: Mathematical and Theoretical* **51**, 125003 (2018).
- ¹²M. E. J. Newman, "Spread of epidemic disease on networks," *Physical Review E* **66**, 016128 (2002).
- ¹³R. M. D'Souza, J. Gómez-Gardenes, J. Nagler, and A. Arenas, "Explosive phenomena in complex networks," *Advances in Physics* **68**, 123–223 (2019).
- ¹⁴R. M. D'Souza and J. Nagler, "Anomalous critical and supercritical phenomena in explosive percolation," *Nature Physics* **11**, 531–538 (2015).
- ¹⁵L. Böttcher and N. Antulov-Fantulin, "Unifying continuous, discrete, and hybrid susceptible-infected-recovered processes on networks," *Physical Review Research* **2**, 033121 (2020).
- ¹⁶J. Fan, J. Meng, Y. Liu, A. A. Saberi, J. Kurths, and J. Nagler, "Universal gap scaling in percolation," *Nature Physics* **16**, 455–461 (2020).
- ¹⁷P. Holme and J. Saramäki, "Temporal networks," *Physics Reports* **519**, 97–125 (2012).
- ¹⁸M. De Domenico, A. Solé-Ribalta, E. Cozzo, M. Kivela, Y. Moreno, M. A. Porter, S. Gómez, and A. Arenas, "Mathematical formulation of multilayer networks," *Physical Review X* **3**, 041022 (2013).
- ¹⁹M. Kivela, A. Arenas, M. Barthelemy, J. P. Gleeson, Y. Moreno, and M. A. Porter, "Multilayer networks," *Journal of Complex Networks* **2**, 203–271 (2014).
- ²⁰C. Berge, *Graphs and Hypergraphs* (North-Holland Pub. Co., Amsterdam, NL, 1973).
- ²¹O. T. Courtney and G. Bianconi, "Generalized network structures: The configuration model and the canonical ensemble of simplicial complexes," *Physical Review E* **93**, 062311 (2016).
- ²²S. Majhi, M. Perc, and D. Ghosh, "Dynamics on higher-order networks: A review," *Journal of the Royal Society Interface* **19**, 20220043 (2022).
- ²³M. S. Anwar and D. Ghosh, "Intralayer and interlayer synchronization in multiplex network with higher-order interactions," *Chaos: An Interdisciplinary Journal of Nonlinear Science* **32**, 033125 (2022).
- ²⁴Z. Wang, M. A. Andrews, Z.-X. Wu, L. Wang, and C. T. Bauch, "Coupled disease-behavior dynamics on complex networks: A review," *Physics of Life Reviews* **15**, 1–29 (2015).
- ²⁵E. P. Fenichel, C. Castillo-Chavez, M. G. Ceddia, G. Chowell, P. A. G. Parra, G. J. Hickling, G. Holloway, R. Horan, B. Morin, C. Perrings, M. Springborn, L. Velazquez, and C. Villalobos, "Adaptive human behavior in epidemiological models," *Proceedings of the National Academy of Sciences* **108**, 6306–6311 (2011).
- ²⁶F. Chen, "A mathematical analysis of public avoidance behavior during epidemics using game theory," *Journal of Theoretical Biology* **302**, 18–28 (2012).
- ²⁷T. C. Reluga, "Equilibria of an epidemic game with piecewise linear social distancing cost," *Bulletin of Mathematical Biology* **75**, 1961–1984 (2013).
- ²⁸L. Böttcher, J. Nagler, and H. J. Herrmann, "Critical behaviors in contagion dynamics," *Physical Review Letters* **118**, 088301 (2017).
- ²⁹F. D. Sahneh and C. M. Scoglio, "Epidemic spread in human networks," in *50th IEEE Conference on Decision and Control and European Control Conference, 11th European Control Conference, CDC/ECC 2011, Orlando, FL, USA, December 12-15, 2011* (IEEE, 2011) pp. 3008–3013.
- ³⁰F. D. Sahneh and C. M. Scoglio, "Optimal information dissemination in epidemic networks," in *Proceedings of the 51th IEEE Conference on Decision and Control, CDC 2012, December 10-13, 2012, Maui, HI, USA* (IEEE, 2012) pp. 1657–1662.
- ³¹H. Shakeri, F. D. Sahneh, C. Scoglio, P. Poggi-Corradini, and V. M. Preciado, "Optimal information dissemination strategy to promote preventive behaviors in multilayer epidemic networks," *Mathematical Biosciences & Engineering* **12**, 609 (2015).
- ³²C. Granell, S. Gómez, and A. Arenas, "Competing spreading processes on multiplex networks: awareness and epidemics," *Physical Review E* **90**, 012808 (2014).
- ³³Q. Guo, X. Jiang, Y. Lei, M. Li, Y. Ma, and Z. Zheng, "Two-stage effects of awareness cascade on epidemic spreading in multiplex networks," *Physical Review E* **91**, 012822 (2015).
- ³⁴V. Sagar, Y. Zhao, and A. Sen, "Effect of time varying transmission rates on the coupled dynamics of epidemic and awareness over a multiplex network," *Chaos: An Interdisciplinary Journal of Nonlinear Science* **28**, 113125 (2018).
- ³⁵M. Scatá, B. Attanasio, G. V. Aiosa, and A. La Corte, "The dynamical interplay of collective attention, awareness and epidemics spreading in the multiplex social networks during COVID-19," *IEEE Access* **8**, 189203–189223 (2020).
- ³⁶Z. Wang, Q. Guo, S. Sun, and C. Xia, "The impact of awareness diffusion on SIR-like epidemics in multiplex networks," *Applied Mathematics and Computation* **349**, 134–147 (2019).
- ³⁷F. Velásquez-Rojas, P. C. Ventura, C. Connaughton, Y. Moreno, F. A. Rodrigues, and F. Vazquez, "Disease and information spreading at different speeds in multiplex networks," *Physical Review E* **102**, 022312 (2020).
- ³⁸J. Fan, Q. Yin, C. Xia, and M. Perc, "Epidemics on multilayer simplicial complexes," *Proceedings of the Royal Society A* **478**, 20220059 (2022).
- ³⁹W. Wang, Q.-H. Liu, J. Liang, Y. Hu, and T. Zhou, "Coevolution spreading in complex networks," *Physics Reports* **820**, 1–51 (2019).
- ⁴⁰M. J. Keeling and B. T. Grenfell, "Understanding the persistence of measles: reconciling theory, simulation and observation," *Proceedings of the Royal Society of London. Series B: Biological Sciences* **269**, 335–343 (2002).
- ⁴¹B. D. Elderder, G. Dwyer, and V. Dukic, "Population-level differences in disease transmission: A Bayesian analysis of multiple smallpox epidemics," *Epidemics* **5**, 146–156 (2013).
- ⁴²L. Böttcher and J. Nagler, "Decisive conditions for strategic vaccination against SARS-CoV-2," *Chaos: An Interdisciplinary Journal of Nonlinear Science* **31**, 101105 (2021).
- ⁴³Y. Zhou, J. Zhou, G. Chen, and H. E. Stanley, "Effective degree theory for awareness and epidemic spreading on multiplex networks," *New Journal of Physics* **21**, 035002 (2019).
- ⁴⁴M. Xia, L. Böttcher, and T. Chou, "Controlling epidemics through optimal allocation of test kits and vaccine doses across networks," *IEEE Transactions on Network Science and Engineering* **9**, 1422–1436 (2022).
- ⁴⁵A.-L. Barabási and R. Albert, "Emergence of scaling in random networks," *Science* **286**, 509–512 (1999).
- ⁴⁶H. Ebel, L.-I. Mielsch, and S. Bornholdt, "Scale-free topology of e-mail networks," *Physical Review E* **66**, 035103 (2002).
- ⁴⁷A.-L. Barabási, H. Jeong, Z. Néda, E. Ravasz, A. Schubert, and T. Vicsek, "Evolution of the social network of scientific collaborations," *Physica A: Statistical mechanics and its applications* **311**, 590–614 (2002).
- ⁴⁸R. Albert, H. Jeong, and A.-L. Barabási, "Diameter of the world-wide web," *Nature* **401**, 130–131 (1999).
- ⁴⁹L. Danon, T. A. House, J. M. Read, and M. J. Keeling, "Social encounter networks: collective properties and disease transmission," *Journal of The Royal Society Interface* **9**, 2826–2833 (2012).
- ⁵⁰C. Brown, A. Noulas, C. Mascolo, and V. Blondel, "A place-focused model for social networks in cities," in *2013 International Conference on Social Computing* (IEEE, 2013) pp. 75–80.
- ⁵¹A. D. Broido and A. Clauset, "Scale-free networks are rare," *Nature Communications* **10**, 1–10 (2019).
- ⁵²K. Bringmann, R. Keusch, and J. Lengler, "Geometric inhomogeneous random graphs," *Theoretical Computer Science* **760**, 35–54 (2019).
- ⁵³G. Ódor, D. Czifra, J. Komjáthy, L. Lovász, and M. Karsai, "Switchover phenomenon induced by epidemic seeding on geometric networks," *Proceedings of the National Academy of Sciences* **118**, e2112607118 (2021).

- ⁵⁴A.-L. Barabási, R. Albert, and H. Jeong, “Mean-field theory for scale-free random networks,” *Physica A: Statistical Mechanics and its Applications* **272**, 173–187 (1999).
- ⁵⁵J. Jorritsma, “Random graph visualizations,” (2020).
- ⁵⁶C.-C. Lai, T.-P. Shih, W.-C. Ko, H.-J. Tang, and P.-R. Hsueh, “Severe acute respiratory syndrome coronavirus 2 (SARS-CoV-2) and coronavirus disease-2019 (COVID-19): The epidemic and the challenges,” *International Journal of Antimicrobial Agents* **55**, 105924 (2020).
- ⁵⁷S. W. Park, B. M. Bolker, D. Champredon, D. J. Earn, M. Li, J. S. Weitz, B. T. Grenfell, and J. Dushoff, “Reconciling early-outbreak estimates of the basic reproductive number and its uncertainty: framework and applications to the novel coronavirus (SARS-CoV-2) outbreak,” *Journal of the Royal Society Interface* **17**, 20200144 (2020).
- ⁵⁸C. Y. Liu, J. Berlin, M. C. Kiti, E. Del Fava, A. Grow, E. Zagheni, A. Melegaro, S. M. Jenness, S. B. Omer, B. Lopman, *et al.*, “Rapid review of social contact patterns during the COVID-19 pandemic,” *Epidemiology* **32**, 781 (2021).
- ⁵⁹H. Xin, Y. Li, P. Wu, Z. Li, E. H. Lau, Y. Qin, L. Wang, B. J. Cowling, T. K. Tsang, and Z. Li, “Estimating the latent period of coronavirus disease 2019 (COVID-19),” *Clinical Infectious Diseases* **74**, 1678–1681 (2022).
- ⁶⁰L. Böttcher, M. Xia, and T. Chou, “Why case fatality ratios can be misleading: individual-and population-based mortality estimates and factors influencing them,” *Physical Biology* **17**, 065003 (2020).
- ⁶¹“Duration of Isolation and Precautions for Adults with COVID-19,” (2020, accessed: January 4, 2021).
- ⁶²H. Salje, C. Tran Kiem, N. Lefrancq, N. Courtejoie, P. Bosetti, J. Paireau, A. Andronico, N. Hozé, J. Richet, C.-L. Dubost, *et al.*, “Estimating the burden of SARS-CoV-2 in France,” *Science* **369**, 208–211 (2020).
- ⁶³L. Böttcher, M. R. D’Orsogna, and T. Chou, “Using excess deaths and testing statistics to determine COVID-19 mortalities,” *European Journal of Epidemiology* **36**, 545–558 (2021).
- ⁶⁴A. Teslya, T. M. Pham, N. G. Godijk, M. E. Kretzschmar, M. C. Bootsma, and G. Rozhnova, “Impact of self-imposed prevention measures and short-term government-imposed social distancing on mitigating and delaying a COVID-19 epidemic: A modelling study,” *PLOS Medicine* **17**, e1003166 (2020).
- ⁶⁵R. Albert, H. Jeong, and A.-L. Barabási, “Error and attack tolerance of complex networks,” *Nature* **406**, 378–382 (2000).
- ⁶⁶R. Cohen, K. Erez, D. Ben-Avraham, and S. Havlin, “Resilience of the Internet to Random Breakdowns,” *Physical Review Letters* **85**, 4626 (2000).
- ⁶⁷R. Cohen, K. Erez, D. Ben-Avraham, and S. Havlin, “Breakdown of the Internet under Intentional Attack,” *Physical Review Letters* **86**, 3682 (2001).
- ⁶⁸D. T. Gillespie, “A General Method for Numerically Simulating the Stochastic Time Evolution of Coupled Chemical Reactions,” *Journal of Computational Physics* **22**, 403–434 (1976).
- ⁶⁹D. T. Gillespie, “Exact Stochastic Simulation of Coupled Chemical Reactions,” *The Journal of Physical Chemistry* **81**, 2340–2361 (1977).
- ⁷⁰L. Böttcher and H. J. Herrmann, *Computational Statistical Physics* (Cambridge University Press, Cambridge, UK, 2021).